LANGMUIR Article
Cite This: Langmuir 2019, 35, 11940−11949
pubs.acs.org/Langmuir

Size-Dependent Interaction of Amyloid β Oligomers with Brain Total Lipid Extract Bilayer—Fibrillation Versus Membrane Destruction

Dusan Mrdenovic,[†,§] Marta Majewska,[†] Izabela S. Pieta,[†] Piotr Bernatowicz,[†] Robert Nowakowski,[†] Wlodzimierz Kutner,[†,‡] Jacek Lipkowski,[§] and Piotr Pieta*[,†]

[†]Institute of Physical Chemistry, Polish Academy of Sciences, Kasprzaka 44/52, 01-224 Warsaw, Poland
[‡]Faculty of Mathematics and Natural Sciences, School of Sciences, Cardinal Stefan Wyszynski University in Warsaw, Wóycickiego 1/3, 01-815 Warsaw, Poland
[§]Department of Chemistry, University of Guelph, 50 Stone Road East, Guelph, Ontario N1G 2W1, Canada

Supporting Information

ABSTRACT: Amyloid β, Aβ(1−42), is a component of senile plaques present in the brain of Alzheimer's disease patients and one of the main suspects responsible for pathological consequences of the disease. Herein, we directly visualize the Aβ activity toward a brain-like model membrane and demonstrate that this activity strongly depends on the Aβ oligomer size. PeakForce quantitative nanomechanical mapping mode of atomic force microscopy imaging revealed that the interaction of large-size (LS) Aβ oligomers, corresponding to high-molecular-weight Aβ oligomers, with the brain total lipid extract (BTLE) membrane resulted in accelerated Aβ fibrillogenesis on the membrane surface. Importantly, the fibrillogenesis did not affect integrity of the membrane. In contrast, small-size (SS) Aβ oligomers, corresponding to low-molecular-weight Aβ oligomers, created pores and then disintegrated the BTLE membrane. Both forms of the Aβ oligomers changed nanomechanical properties of the membrane by decreasing its Young's modulus by ∼45%. Our results demonstrated that both forms of Aβ oligomers induce the neurotoxic effect on the brain cells but their action toward the membrane differs significantly.

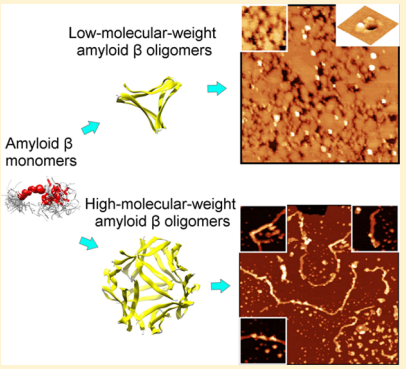

INTRODUCTION

Alzheimer's disease (AD) involves progressive neurodegeneration that includes symptoms such as dementia, memory loss, and communication difficulties.[1] AD belongs to the group of so-called protein misfolding diseases, that is, diseases associated with misfolded forms of proteins.[2] Parkinson's disease and Huntington's disease are two examples of these diseases.[2] Hallmarks of AD are manifested in patients' brains as intra- and extracellular protein deposits called neurofibrillary tangles and amyloid (senile) plaques, respectively. Amyloid β (Aβ) peptide is the major component of the amyloid plaques.[3] The proteolytic cleavage of transmembrane protein, called amyloid precursor protein, by β- and γ-secretase cleaving enzymes leads to the formation of 38−43 (amino acid)-long Aβ peptide.[4] From the AD perspective, peptides composed of 40 (Aβ40) and 42 (Aβ42), amino acids are the most relevant. The Aβ40 is the predominant form. However, the Aβ42 is more toxic, has higher aggregation propensity, and its concentration in body fluids of AD patients is elevated.[5]

The Aβ has the tendency of nucleation-dependent aggregation, a process leading to fibrillogenesis (fibrillation).[6] In this process, single monomers aggregate into low-molecular-weight (LMW) oligomers, then into high-molecular-weight (HMW) oligomers forming either globular oligomers or elongated protofibrils, and finally mature fibrils.[7] Fibrillation is a complex process that not only involves aggregation but also fragmentation of the aggregates. As a result, Aβ oligomers of different molecular weights are in equilibrium. Each of the Aβ oligomer forms shows different levels of toxicity toward neuronal cells. However, there is no agreement which form of oligomers is the most toxic and what is the mechanism of Aβ toxicity. The most popular mechanisms include pore/ion channel formation,[8,9] membrane fragmentation/lipid extraction,[10,11] and membrane thinning.[12,13] It is not clear whether one or combination of several proposed mechanisms are concertedly engaged in this toxicity. Moreover, it is unknown which form of oligomers is responsible for these mechanisms. Some studies suggest that the Aβ aggregation itself is toxic.[6,14] Because the aggregation rate is increased on surfaces of cell membranes or amyloid fibrils,[15,16] rapid aggregation might be another reason for neuronal damage encountered in the AD patients.

Deep knowledge of the brain cell death mechanism caused by various forms of Aβ42 oligomers is crucial for understanding of AD and developing an appropriate treatment. The objective of the present study is to elucidate mechanisms of the

Received: May 31, 2019
Revised: July 18, 2019
Published: July 21, 2019

DOI: 10.1021/acs.langmuir.9b01645
Langmuir 2019, 35, 11940−11949

Aβ oligomer toxicity. In our research, we simulated the interaction of Aβ42 (in brief referred as Aβ) oligomers with a model human cell membrane. We introduced Aβ oligomers of a controlled size and concentration to the suspension of small unilamellar vesicles (SUVs) composed of phospholipids whose composition is representative for the brain cell membranes. Then, we deposited the fused SUVs on a mica substrate, which ruptured and formed a model cell membrane. We examined effectiveness of the Aβ action toward SUVs by unraveling changes in the topography and nanomechanical properties of the model membrane interacting with Aβ by atomic force microscopy (AFM). This examination allowed us to identify the mechanisms of action of Aβ oligomers of different size. AFM studies showing the Aβ interaction with model cell membranes have already been performed,[9,17,18] however, our present results provide unique information allowing one to distinguish between the mechanisms of toxic interactions of small-size (SS) and large-size (LS) Aβ oligomers with the model membrane. SS and LS oligomers correspond to LMW and HMW oligomers, respectively. Herein, we present high-resolution AFM images showing LS Aβ oligomer fibrillation through both primary and secondary nucleation mechanism on the brain total lipid extract (BTLE) vesicle surface, without affecting the membrane integrity. On the other hand, SS Aβ oligomers destroyed the BTLE membrane by combination of the pore formation and lipid extraction mechanisms.

EXPERIMENTAL SECTION

Aβ Peptide Preparation. Lyophilized Aβ(1−42), named Aβ, was purchased from Bachem (Bubendorf, Switzerland). Its purity was determined to be 92% using ^{1}H NMR spectroscopy (Figure S1, Supporting Information). The Aβ sample was pretreated by following the earlier developed procedure[19] illustrated in Figure S2 in the Supporting Information.

To break pre-existing aggregates, 1 mg of Aβ was dissolved in 1 mL of trifluoroacetic acid (TFA), then sonicated for 15 min in a cold water bath followed by solvent evaporation under Ar stream. Next, the sample was dissolved in 1 mL of 1,1,1,3,3,3-hexafluoro-2-propanol (HFIP) from Sigma-Aldrich, then sonicated for 10 min, and then HFIP was removed under Ar stream. HFIP addition, sonication, and solvent removal were repeated once more, and then 1 mL of HFIP was added for the third time. The sample was stored for 24 h at 4 °C. Next, the sample was vortexed for 5 min, and then aliquoted. Afterward, HFIP was evaporated under Ar stream, which resulted in clear Aβ films left on the bottom of centrifuge tubes. Residual HFIP was removed from the films under reduced pressure in a desiccator for 1 h. The films were stored at −80 °C in a freezer. For each experiment, an aliquot taken from the freezer was allowed to equilibrate to room temperature (RT) for 15 min. Next, the Aβ film was dissolved in anhydrous dimethyl sulfoxide (DMSO) from Sigma-Aldrich to reach the 5 mM concentration, and then further diluted to the 10 μM concentration using 0.01 M phosphate buffer saline, PBS, (pH = 7.4) solution from Sigma-Aldrich. Before use, this solution was filtered through the Whatman syringe filter (GE Healthcare Life Sciences) of 0.02 μm porosity.

Size of the Aβ oligomers was controlled by varying their aggregation time in the mixed solvent solution of 0.01 M PBS (pH = 7.4) and anhydrous DMSO. Size distribution of the Aβ oligomers was characterized by depositing 5 μL of 5 μM Aβ solution on mica. After subsequent washing with Milli-Q water (18.2 MΩ cm) and drying, the sample was AFM imaged in air.[20−22]

BTLE-Supported Lipid Bilayer Preparation. A chloroform solution of the porcine BTLE was purchased from Avanti Polar Lipids and used without further purification. Supported lipid bilayers (SLBs) were prepared using the vesicle fusion method.[23] The BTLE vesicle solution was prepared by transferring 4 μL of the BTLE stock solution in chloroform (25 mg mL^{-1}) to a glass vial followed by solvent evaporation with Ar stream, accompanied by vortexing until a dry film appeared on the bottom of the vial (Figure S2, Supporting Information). After solvent evaporation, the lipid film was dried in desiccator overnight. Then, it was resuspended in a filtered PBS solution (pH = 7.4) to reach the 1 mg mL^{-1} concentration, and subsequently sonicated for 20 min at 40 °C. The BTLE vesicle solution was used either immediately or stored at 4 °C until further use.

To study the BTLE bilayer in the Aβ absence, a 40 μL sample of the BTLE vesicle solution was dropcast on the mica surface, and then left for 45 min to allow for the bilayer formation. Next, the sample was washed with filtered Milli-Q water, then immersed in the PBS (pH = 7.4) solution, and immediately imaged with AFM.

Aβ−BTLE Mixture Preparation. The SS or LS Aβ oligomers were mixed with that of BTLE vesicles at the 1:20 or 1:50 peptide-to-lipid mass ratio (Figure S2, Supporting Information). Then, the mixture was sonicated for 10 min at RT. To study the time-dependent mechanism of the Aβ−BTLE vesicle interaction, 40 μL aliquots of the Aβ−BTLE mixture were sampled at different time intervals, and dropcast on the mica surface. After 45 min, the sample was rinsed with Milli-Q water, immersed in the PBS (pH = 7.4) solution, and immediately imaged.

The DMSO solvent can cause membrane thinning, pore formation, and membrane disintegration.[24,25] In the present studies, the DMSO concentration in the presence of the lipid bilayer was 0.1% (v/v). At this low concentration, DMSO has no adverse effect neither on the stability nor topography of the lipid bilayer, (Figure S3a in Supporting Information). For control measurements, a sample of the supported BTLE bilayer in the AFM liquid cell was prepared, and then imaged. After acquiring images of an intact BTLE membrane, 40 μL of ∼5 μM SS Aβ solution was added to the solution. This concentration of SS oligomers corresponds to concentration of Aβ in the Aβ−BTLE vesicle mixtures. Next, the AFM cell was filled with the PBS (pH = 7.4) solution, and immediately imaged with AFM.

AFM Experiments. AFM with MultiMode 8 system (Bruker) equipped with E scanner (scan size 10 × 10 μm^2) and the PeakForce quantitative nanomechanical mapping (PF-QNM) mode was used for imaging samples in liquid (PBS solution, pH = 7.4) , at 21 °C. The ScanAsyst mode was used for imaging in air. Before the imaging, the fluid cell and AFM accessories were cleaned in a detergent bath, followed by consecutive rinsing with ethanol, and then Milli-Q water. The V1 grade mica disks (Ted Pella, Inc.) were mounted on metallic disks using an adhesive tape. Just before sample deposition, mica was cleaned in ethanol, and then in Milli-Q water. After drying with Ar stream, its top layer was piled off using an adhesive tape, thus resulting in a clean and atomically flat surface. The qp-BioAC (Nanosensors) and RTESPA300 (Bruker) cantilevers of 0.1 and 40 N m^{-1}, respectively, spring constant and corresponding resonance frequency of 50 and 300 kHz, respectively, were used for imaging in liquid and in air, respectively. The AFM cantilevers were cleaned by consecutive immersing in a detergent bath, 2-propanol, and Milli-Q water for 10 min. Next, the cantilevers were ozonized in the UVC-1014 UV ozone cleaner (Nanobioanalytics, Berlin, Germany) for 10 min. The cantilevers were calibrated using the thermal tune method. The tip radius was determined by imaging the Ti roughness sample (Bruker), routinely used for tip radius determination.[26,27] The PF-QNM images were obtained using a 1−2 Hz scan rate. Images were processed and analyzed using NanoScope analysis of Bruker and Gwyddion software.[28]

Nanomechanical Property Analysis. Data were analyzed using AtomicJ software.[29] The contact point was found on the extended curve. All Young's modulus (YM) fitting was performed on the retraction curve using the Hertz model.

NMR Spectroscopy Study. Purity of the Aβ sample was assessed with ^{1}H NMR spectroscopy. For that, first, 1 mg of Aβ was dissolved in 1 mL of deuterated TFA (TFA-*d*), then sonicated for 15 min at RT, and then subjected to the NMR spectroscopy analysis. The latter was performed at 298 K using Bruker AVANCE II 300 MHz spectrometer. At first, longitudinal relaxation times (T_1) of ^{1}H nuclei were determined using the inversion-recovery technique[30] to be

DOI: 10.1021/acs.langmuir.9b01645
Langmuir 2019, 35, 11940−11949

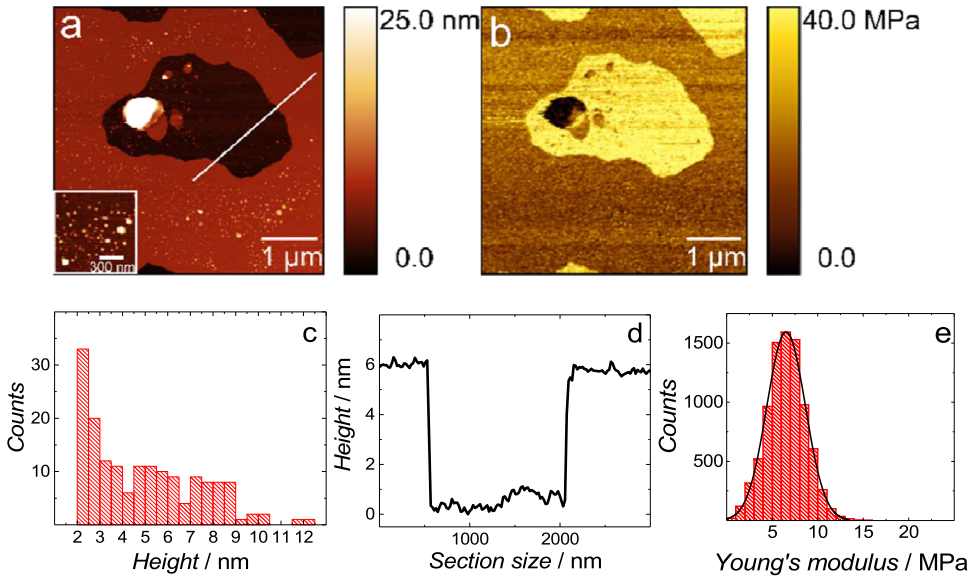

Figure 1. (a) The AFM topography image and (b) the corresponding YM map of the BTLE bilayer with adsorbed LS Aβ oligomers deposited on mica immediately after mixing solutions of LS Aβ oligomers and BTLE vesicles. Inset in Panel a exhibits a magnified section of the same topography image showing the shape of the LS Aβ oligomers on the membrane surface. The images were acquired for the bilayer in the PBS (pH = 7.4) solution at 21 °C. (c) Height distribution of the LS Aβ oligomers determined from the AFM image shown in Panel a. (d) Cross-sectional profile measured along the line shown in Panel a, exhibiting the BTLE bilayer thickness. (e) Histogram showing the YM distribution determined from 6000 FD curves collected for different points of the BTLE bilayer shown in Panel b.

between 20 and 180 ms. Then, the quantitative ^{1}H NMR spectrum of high quality was acquired with 2048 scans. The recycle delay between scans was 2 s to avoid signal oversaturation. The pulse duration was 11.7 μs, spectral width was 7.5 kHz, and the acquisition time was 2.2 s. Before integration, the spectrum was carefully phased and subjected to baseline correction in order to avoid integral distortion.

RESULTS AND DISCUSSION

AFM Characterization of the BTLE Bilayer without Aβ. The PF-QNM mode of AFM was employed to study topography and nanomechanical properties of the supported BTLE bilayer deposited on the mica surface. The topography image of the BTLE bilayer supported on the mica surface is shown in Figure S3a in Supporting Information. The surface of this bilayer was smooth without defects or discontinuities. Average thickness of this bilayer, determined by height profiling along the line shown in Figure S3a, was 6.1 (±0.3) nm (Figure S3c, Supporting Information). This thickness is in agreement with a typical height of the SLBs.[31,32] Figure S3b in Supporting Information shows the YM map, determined from the FD curves acquired simultaneously with the topography imaging. YM was determined by fitting the Hertz model to the retracted part of the FD curves.[29] This model is described by

$$F = \frac{4E}{3(1-\nu)}\sqrt{R}\,\delta^{3/2} \quad (1)$$

where F is the load applied, E is YM, ν is the Poisson's ratio, δ is the depth of indentation, and R is the AFM tip radius. Figure S3d in Supporting Information shows YM distribution of the bilayer shown in Figure S3a in Supporting Information. This distribution is narrow, thus confirming membrane homogeneity, with the average modulus value of 11.8 (±3.2) MPa.

AFM Characterization of Aβ Oligomers. Different forms of Aβ oligomers induce different levels of cell toxicity.[33−36] Hence, the mechanism of the Aβ interaction with a cell membrane should depend on the molecular weight of Aβ. Therefore, Aβ samples with different size distributions were prepared. Because the molecular weight of the studied Aβ oligomers was not measured, the LMW and HMW oligomers were distinguished only on the basis of their size (SS or LS oligomers, respectively). Initially (0 h aggregation time, Figure S2, Supporting Information), freshly prepared samples of 10 μM Aβ in a PBS−DMSO mixture were analyzed to confirm that pre-existing aggregates were eliminated and those monomers of Aβ were the predominant form in the sample. An aliquot of this solution was deposited on the mica substrate. After 5 min deposition, the sample was washed, then dried under Ar stream, and the immediately imaged by AFM in air. Figure S4a in Supporting Information shows many globular aggregates on the mica surface. Statistical analysis of the sample revealed that these aggregates with the height of ∼0.7 nm and average diameter of ∼2 nm populate the most abundant fraction and only a minor number of SS Aβ oligomers were distinguished (Figures S4d and S8a, Supporting Information). This height corresponds to the height of the Aβ monomer.[37,38] At this stage, monomers and SS oligomers are in equilibrium.[39,40] After establishing monomers to be predominant in a freshly prepared sample, the fibrillogenesis was monitored as a function of the aggregation time. First, Aβ was allowed to aggregate for 24 h at 4 °C. At this point, the Aβ aggregated and SS Aβ oligomers with 1.5−2.5 nm height and average diameter of ∼6 nm were the most dominant (Figures S4b,e and S8b, Supporting Information). After 48 h, Aβ aggregation progressed further to result in both the SS and LS oligomers (Figure S4c, Supporting Information). Statistical analysis of the height of the Aβ aggregates generated after 48 h aggregation resulted in bimodal distribution of aggregates with the height of 1−2.5 (19.64%) and 3−6 nm (80.36%) corresponding to the SS and LS Aβ oligomers, respectively (Figure S4f, Supporting Information). Average diameter of newly formed LS Aβ oligomers was ∼10 nm. These sizes of Aβ oligomers are in agreement with those determined by

DOI: 10.1021/acs.langmuir.9b01645
Langmuir 2019, 35, 11940−11949

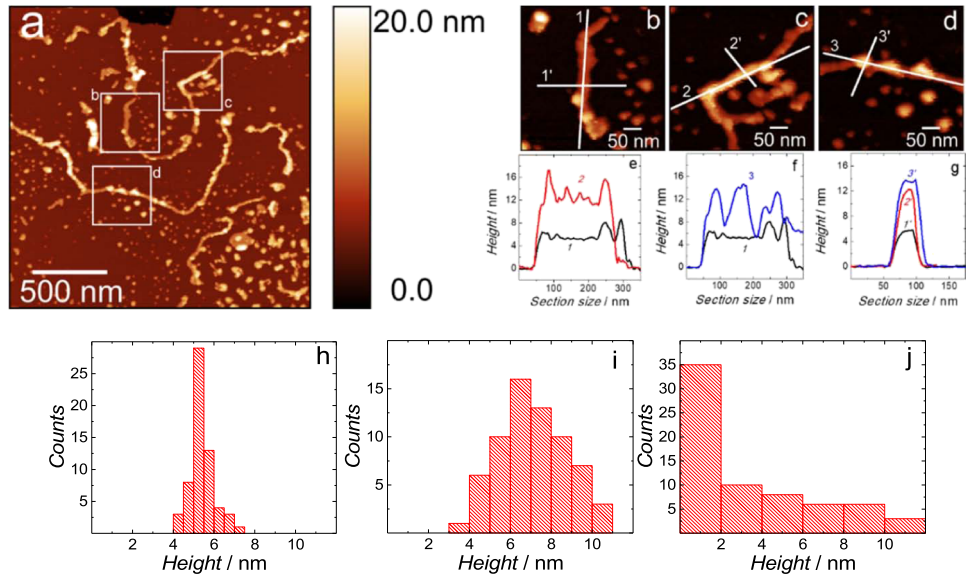

Figure 2. (a) The AFM topography image of the Aβ aggregates formed on the BTLE-supported bilayer in 0.01 M PBS (pH = 7.4). (b–d) High-resolution topography images, acquired for the areas depicted as squares in Panel a, showing the (b) primary nucleation fibril, (c) secondary nucleation fibril, and (d) secondary nucleation globular aggregates. (e–g) Cross-sectional profiles measured along (e) the primary and the secondary nucleation fibrils (lines 1 and 2) and (f) primary nucleation fibril and secondary nucleation globular aggregate (lines 1 and 3) as well as (g) across the primary and secondary nucleation aggregates (lines 1′, 2′ and 3′). (h–j) Histograms showing the height distribution of (h) primary nucleation fibrils, (i) secondary nucleation fibrils, and (j) secondary nucleation globular aggregates of Aβ.

AFM,[34,36,38,40,41] dynamic light scattering (DLS),[34] fluorescence correlation spectroscopy,[34] and transmission electron microscopy (TEM).[40,41] Their corresponding molecular weights were determined by electrophoresis[36,38,41] and MALDI-TOF.[40] Using the abovementioned literature, one may roughly estimate that oligomers with the height of 1–2.5 nm correspond to trimers and tetramers with the molecular weight of ~30 kDa.[38] Most likely, the molecular weight of Aβ forms with the height of 3–6 nm exceeds ~60 kDa, which is that of a dodecamer.[38] Noteworthy, Aβ aggregates similar in shape and size were extracted from amyloid plaques of AD patient brains.[42] Interestingly, only globular aggregates were formed if the aggregation time was shorter than 48 h. However, protofibrils and fibrils of Aβ were observed if the aggregation time exceeded 48 h, (Figure S5, Supporting Information).

Interaction of LS Aβ Oligomers with BTLE Vesicles. The PF-QNM AFM technique was employed to study the Aβ–BTLE vesicle interaction. The LS Aβ oligomer solution was mixed with the BTLE vesicle solution at the Aβ-to-lipid mass ratio of 1:20. In order to monitor the time-dependent interaction of LS Aβ oligomers with BTLE vesicles, 40 μL aliquots of the mixture were taken at different interaction times and dropcast onto the mica surface. The vesicles were allowed to fuse for 45 min, then the sample was carefully washed with filtered Milli-Q water, and then imaged in PBS (pH = 7.4) solution. Figure 1a shows the AFM image of the Aβ–BTLE bilayer deposited after mixing solutions of LS Aβ oligomers and the BTLE vesicle solution (0 h interaction time). The image shows many globular Aβ aggregates on the BTLE bilayer surface. The height distribution of these aggregates exceeded 3 nm (Figure 1c), which indicates that these were mostly LS Aβ oligomers. A comparison of the height distribution of Aβ aggregates formed in solution in the absence (Figure S4f, Supporting Information) and in the presence (Figure 1c) of BTLE vesicles shows that the BTLE vesicles promoted large Aβ oligomer growth on the membrane surface. Moreover, the aggregation rate was significantly increased in the presence of the BTLE surface. Both the phospholipid composition and the presence of cholesterol decreased the half time of Aβ aggregation.[43,44] Apparently, the BTLE bilayer is a very efficient catalyst of LS oligomers aggregation. This conclusion is consistent with previous studies showing the catalytic role of lipid bilayers on amyloid fibrillation by ThT fluorescence,[43] Förster resonance energy transfer assay,[43] circular dichroism,[45] NMR spectroscopy,[45] X-ray scattering,[46] neutron reflectivity,[46] TEM,[46] DLS,[46] and AFM.[43]

The cross-sectional profile (Figure 1d) showed that thickness of the BTLE bilayer exposed to LS Aβ oligomers was 5.9 (±0.2) nm, which is similar to the BTLE thickness in the absence of Aβ (Figure S3c, Supporting Information). Nanomechanical properties of the BTLE bilayer with adsorbed LS Aβ oligomers were significantly different from those of the intact bilayer. Figure 1b shows the YM map corresponding to the topography image shown in Figure 1a. Distribution of the YM (Figure 1e) showed the average value of 6.5 (±2.5) MPa, which is half of that determined for the intact bilayer (Figure S3d).

Interestingly, many Aβ fibrils were formed on the BTLE membrane surface after 3 h of Aβ–BTLE vesicle interaction (Figure 2a). Additionally, other objects are visible on the fibril surface forming both individual globular aggregates and long fibrillary structures. It suggests that the secondary nucleation mechanism of Aβ aggregation was observed. Aggregation through secondary nucleation is unique and can be distinguished from other steps in the aggregation pathway because it is the only step that occurs on top of already formed Aβ fibrils.[44,47] This process is a surface reaction involving coalescence of Aβ aggregates rather than a result of their deposition from the solution bulk. The presence of the secondary nucleation aggregates is clearly seen in Figure 2c,d. Herein, the aggregation through secondary nucleation resulted in the formation of fibrillary (Figure 2c) and globular Aβ

DOI: 10.1021/acs.langmuir.9b01645
Langmuir 2019, 35, 11940–11949

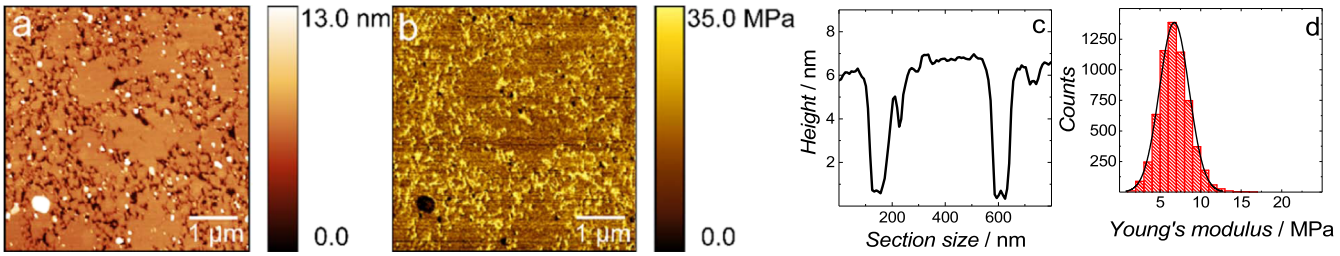

Figure 3. (a) The AFM topography image and (b) the corresponding YM map of the Aβ−BTLE supported bilayer in 0.01 M PBS (pH = 7.4), at the initial interaction time. (c) The representative cross-sectional profile showing depth of the pores in the BTLE lipid bilayer depicted in Panel a. (d) Histogram showing the YM distribution determined from 6000 FD curves acquired for different points of the bilayer shown in Pnel b.

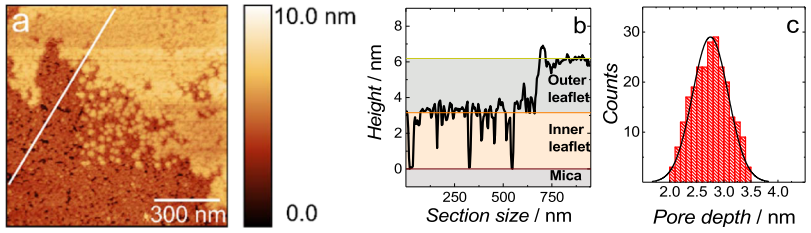

Figure 4. (a) The topography image of the Aβ−BTLE supported bilayer in 0.01 M PBS (pH = 7.4) showing lipid extraction from the outer leaflet of the BTLE bilayer. (b) The corresponding height profile, measured along the line in Panel a, showing the height difference between the outer and inner leaflet of the BTLE lipid bilayer. (c) Histogram showing the depth distribution of the pores formed in the inner leaflet of the BTLE bilayer.

aggregates (Figure 2d) on top of the Aβ fibrils preformed through primary nucleation. To compare heights of the Aβ fibrils formed through primary and secondary nucleation, cross-sectional profiles along and across the aggregates were recorded and analyzed (Figure 2e−g). Figure 2h−j shows the corresponding heights histograms. A narrow Gaussian distribution of heights for the primary nucleation fibrils indicates that their average height was 5.4 (±0.6) nm (Figure 2h). In contrast, a wide height distribution was observed for the secondary nucleation fibrils with an average height of 7.09 (±1.62) nm (Figure 2i). Height distribution of globular aggregates formed through secondary nucleation was quite wide covering the range of 1−12 nm (Figure 2j). The height of the larger population of secondary globular aggregates was 1−2 nm, which corresponds to the height of SS Aβ oligomers. This is not surprising because the SS Aβ oligomers aggregate to form fibrils. Notably, LS Aβ oligomers seen at the initial interaction time (Figure 1a) were also visible after 3 h of interaction with the BTLE vesicles (Figure 2a). The LS Aβ oligomers aggregation into fibrillar aggregates was much faster in the presence of the BTLE membrane. Therefore, we can conclude that aggregates observed directly on the membrane surface were formed during aggregation catalyzed by the membrane surface, which occurred via the primary nucleation mechanism. The aggregates observed on the fibril surface were formed during aggregation catalyzed by the fibril surface, which is the secondary nucleation mechanism.[44,47]

Interaction of SS Aβ Oligomers with BTLE Vesicles. Exposure of SS Aβ oligomers to BTLE vesicles (the Aβ-to-lipid mass ratio of 1:20) resulted in deposition of the Aβ−BTLE bilayer, which significantly differed from that shown in Figure 1. Figure 3a shows the Aβ−BTLE film deposited on the mica substrate immediately after mixing solutions of SS Aβ oligomers and BTLE vesicles. There were numerous pores of different sizes and shapes on the surface of the resulting BTLE bilayer. Long fibrils or large globular aggregates, previously seen in Figures 1a and 2a, were absent. Clearly, the interaction of SS Aβ oligomers with BTLE vesicles resulted in vesicles spreading differently than that described above for LS Aβ oligomers. The cross-sectional profile of the membrane shown in Figure 3a indicates that the BTLE film thickness was 6.3 (±0.6) nm (Figure 3c), a value comparable to that of the intact BTLE bilayer (Figure S3c, Supporting Information).

Figure 3b shows the YM map corresponding to the topography image shown in Figure 3a. The average YM distribution of this bilayer was 6.7 (±2.2) MPa (Figure 3d), a value comparable to that of the membrane with adsorbed LS Aβ oligomers. Therefore, the presence of both LS and SS Aβ oligomers effectively changed nanomechanical properties of the BTLE membrane by causing a decrease of YM by ∼45%. Force spectroscopy measurements revealed that the POPC/POPS SLB ruptured in the absence and presence of the Aβ42 at 3.5 and 1.2 nN, respectively, thus indicating a 65.71% decrease in the bilayer stiffness.[18] This significant membrane nanomechanical property change incurred by the Aβ activity implies both conformational and organizational changes of the phospholipid molecules in the membrane.

We repeatedly observed porous bilayer formation from BTLE vesicles with SS Aβ oligomers (Figure 3a). Occasionally, we recorded images showing partial BTLE bilayer formation (Figure 4a). The film shown in Figure 4a features numerous pores in both the outer and inner leaflet of the BTLE bilayer. The cross-sectional profile, measured along the line shown in Figure 4a, exhibits equal height of the outer and inner leaflet to be ∼3.1 nm (Figure 4b). Average distribution depth of the pores formed in the inner leaflet was 2.8 (±0.4) nm (Figure 4c). Only pores of the diameter bigger than the diameter of the AFM tip were considered in this analysis. The AFM tip characterization is provided in Figures S6 and S7 in Supporting Information. These results show that the bottom leaflet of the film has thickness of a monolayer and only a part of the upper leaflet is present forming a complete bilayer.

Our AFM studies demonstrated that SS Aβ oligomers have an adverse effect on BTLE vesicles spreading and bilayer forming. The partial absence of the membrane outer leaflet shown in Figure 4a suggests that SS Aβ oligomers induced

DOI: 10.1021/acs.langmuir.9b01645
Langmuir 2019, 35, 11940−11949

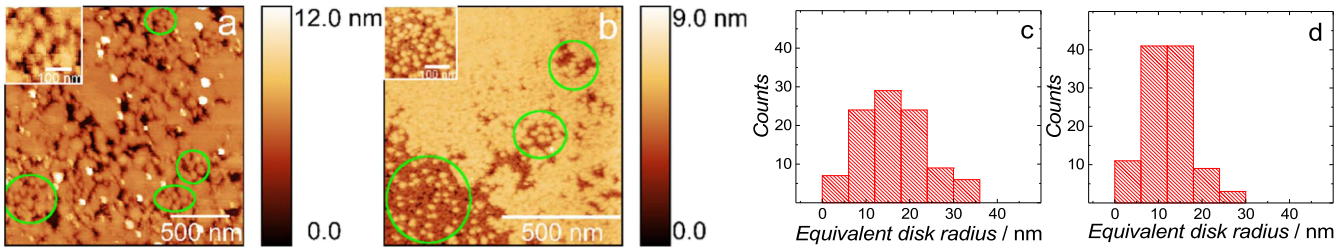

Figure 5. AFM topography images showing nanoclusters (green circled) formed by the BTLE lipids interacting with SS Aβ oligomers in the cases of (a) Figure 3 and (b) Figure 4. Insets exhibit high-resolution AFM topography images showing size and shape of the Aβ–lipid nanoclusters. (c, d) Histograms showing equivalent disk radii distributions of the Aβ–lipid nanoclusters in the cases of (c) Figure 3a and (d) Figure 4b. In order to show sufficient number of nanoclusters, images presented in Panels a and b are of different scan sizes.

extraction of the phospholipid molecules from this leaflet. Aβ oligomers are known to uptake lipid molecules, thus inducing lipid extraction from, for example, a neuronal membrane.[10,11,48−51] Only SS Aβ oligomers (dimers, trimers and tetramers) can extract phospholipid molecules from neuronal cells, thus forming Aβ–lipid complexes, named lipoprotein particles.[48] Moreover, the Aβ–(lipid vesicles) interaction resulted in lipoprotein complex formation.[10,11,50,51] Importantly, these complexes diffuse away from neuronal cells. Lipid extraction is intensified by the increase of the Aβ concentration, the Aβ–cell interaction time, and it depends upon cell membrane composition.[10,50,51] The present studies suggest that the adverse effect of SS Aβ oligomers on BTLE vesicle spreading may result from the lipoprotein complex formation.

Figure 5a,b presents images of the samples shown above in Figures 3a and 4a, respectively, with the globules marked with green circles. Equivalent disk radii distributions of these objects are reported in Figure 5c,d, respectively. The most dominant populations of globules are characterized by the radius between 10 and 20 nm. A similar size of the globules suggests the formation of similar nanoclusters. To verify if the observed nanoclusters are either Aβ aggregates or unfused BTLE vesicles, equivalent disk radii of all globular Aβ forms as well as unruptured BTLE vesicles were measured and compared (Figure S8, Supporting Information). Equivalent disk radii of the Aβ monomers, SS Aβ oligomers, LS Aβ oligomers, and unfused BTLE vesicles were in the range of ∼1, 2−4, 4−6, and 40−80 nm, respectively. Significant difference in the nanocluster radii (Figure 5c,d) compared to that of globular Aβ forms and BTLE vesicles (Figure S8a−d), confirms that the nanoclusters are unique entities. These nanoclusters were observed only in the presence of SS Aβ oligomers, thus suggesting that they correspond to the Aβ–lipid complexes.

Temporal Changes of the Bilayer Formed by Fusion of a Mixture of BTLE Vesicles and SS Aβ Oligomers. In order to detect temporal changes in the bilayer formed by fusion of a mixture of BTLE vesicles and SS Aβ, the mixture of the Aβ-to-lipid mass ratio of 1:50 was used. It allowed for direct imaging of individual pores formed by SS Aβ oligomers. Similar measurements for LS Aβ were not performed because the decrease of the LS oligomer concentration should only affect the aggregation rate.[52] The aggregation rate is directly correlated to the Aβ concentration, that is, the higher the concentration, the higher the aggregation rate. Figure 6 shows the time-lapse AFM imaging of a single pore formed in the Aβ–BTLE bilayer deposited on the mica surface from the mixture of SS Aβ oligomers and BTLE vesicle solutions. Low-

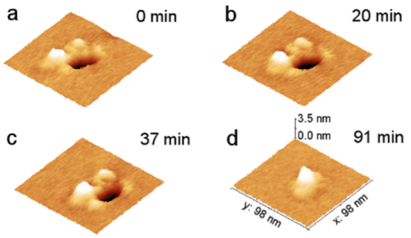

Figure 6. Time-resolved AFM topography images of a single pore in the outer BTLE leaflet formed in 0.01 M PBS (pH = 7.4) by the SS Aβ oligomers after (a) 0, (b) 20, (c) 37, and (d) 91 min.

resolution AFM images are shown in Figure S9 in Supporting Information. The Aβ aggregates surrounding the pores protruded by ∼1 nm above the BTLE membrane surface (Figure S10b, Supporting Information). This protrusion is much lower than that observed for LS Aβ oligomers (Figure 1c). Moreover, equivalent disk radii of the Aβ aggregates, shown in Figure 6, ranged between 2.4 and 4.2 nm being the same as those for SS Aβ oligomers (Figure S8b, Supporting Information), thus suggesting that the pores were formed by SS Aβ oligomers. Pores in the BTLE bilayer were surrounded by a different number of Aβ oligomers. For instance, Figure S10a in the Supporting Information shows the AFM image of eight Aβ oligomers surrounding the pore in the membrane. Within the first ∼37 min, the pore expanded (Figure 6a−c), and then Aβ oligomers entered the pore, thus clogging it (Figure 6d and Movie S1, Supporting Information). The imaged pore filled with SS Aβ oligomers did not change during next 90 min. This behavior was observed repeatedly. Similar behavior was observed for multiple pores. Movie S2 in Supporting Information shows that all pores initially expanded and, eventually, were filled by SS Aβ oligomers. Penetration of the membrane by SS Aβ oligomers and their subsequent insertion into the cell can trigger cell death via leakage of lysosomal enzymes,[53] inhibition of mitochondrial activity,[54] increased production of reactive oxygen species,[55] or cytosolic proteasome impairment.[56] Evidently, exposure of the BTLE membrane to SS Aβ oligomers resulted in membrane poration and subsequent SS Aβ oligomer insertion in the BTLE bilayer, thus leading to bilayer destruction. In detail, first, SS Aβ oligomers form pores in the BTLE membrane. Then, the pores expand over time and SS Aβ oligomers insert themselves into the pores. Once inside the bilayer, these oligomers have access to hydrophobic acyl chains of the BTLE membrane. Aβ oligomers have hydrophobic residues allowing for the hydrophobic–hydrophobic interaction of SS Aβ oligomers with BTLE lipids allowing for nanocluster (Aβ-lipid complex)

DOI: 10.1021/acs.langmuir.9b01645
Langmuir 2019, 35, 11940−11949

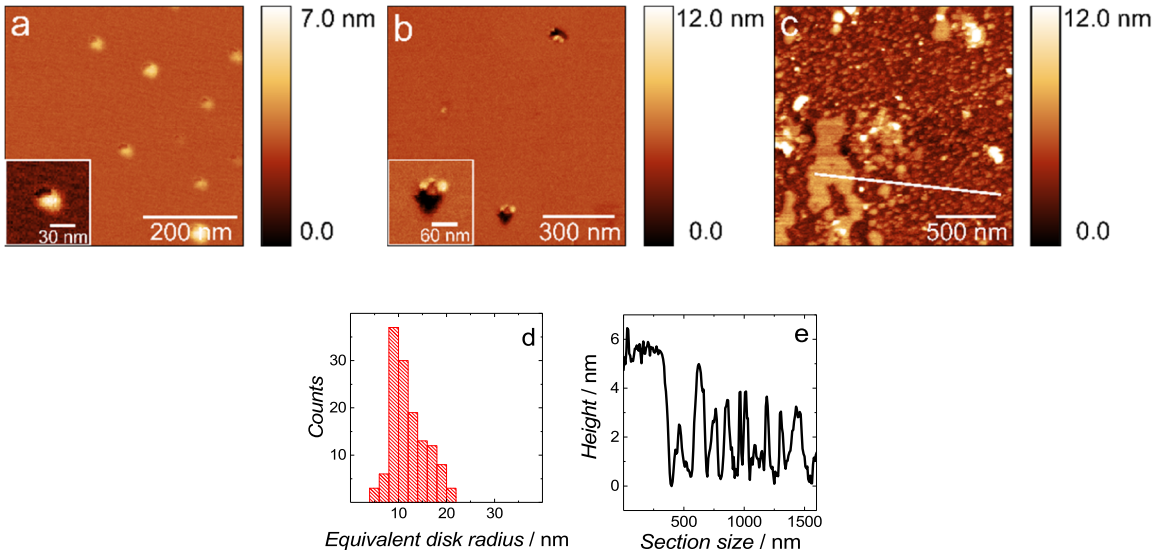

Figure 7. AFM topography images of the supported BTLE bilayer, in 0.01 M PBS (pH = 7.4), exposed to the SS Aβ oligomers for (a) 0, (b) 24, and (c) 72 h. (d) Histogram showing disk radii distribution of the nanoclusters observed in the AFM image in Panel c. (e) The corresponding height profile showing thickness of the supported BTLE bilayer exposed to SS Aβ oligomers for 72 h shown in Panel c.

formation. Hiding hydrophobic parts and exposing hydrophilic parts of both nanocluster components to the solvent increase stability of the Aβ–lipid complexes in the polar environment.

Interaction of SS Aβ Oligomers with BTLE Bilayer Supported on Mica. In order to understand the effect of SS Aβ oligomers on BTLE vesicles, additional measurements were performed. These measurements, named as the control measurements, were performed to understand whether the topography changes in the BTLE bilayers (Figures 3a and 4a) were due to SS Aβ activity or ineffective disruption and fusion of vesicles. The control measurements for the LS Aβ oligomers were not performed because the AFM images shown in Figures 1a and 2a clearly indicated the presence LS Aβ oligomers on the membrane surface and their mechanism of interaction with the BTLE bilayer. The bilayer was first deposited on mica, and then exposed to SS Aβ oligomers. For this purpose, 40-μL sample of ~5 μM SS Aβ solution was added to the AFM cell. This concentration of SS oligomers corresponds to concentration of Aβ in the Aβ–BTLE vesicle mixtures. Figure 7 shows a sequence of AFM images acquired for the supported BTLE bilayer interacting with SS Aβ oligomers for different time lapses. Initially, only single Aβ oligomers, protruding 2–3 nm above the bilayer plane were observed (Figure 7a). Around these oligomers, small (0.5 nm deep) pores were present (inset in Figure 7a). After 24 h, there were pores with the radius and depth of ~22 and ~5 nm, respectively (Figure 7b). Inset to Figure 7b shows that SS Aβ oligomers were present at the edges of these pores. Therefore, the pore depth increased from 0.5 to 5 nm after 24 h exposure of the BTLE membrane to SS Aβ oligomers. The bilayer was almost completely disintegrated after 72 h (Figure 7c). Numerous globular objects with disk radii of 10–20 nm (Figure 7d) and remnants of the 5.7 nm thick bilayer (Figure 7e) were seen. For comparison, intact supported BTLE bilayer imaged after 0 and 72 h is shown in Figure S11 in Supporting Information. Apparently, the bilayer was stable for 3 days and its disintegration shown in Figure 7 results from the interaction with the SS Aβ oligomers. The globular objects observed in Figure 7c were of the size comparable to that of globules shown in Figure 5a,b. This suggests that porous bilayer formation by spreading of a mixture of BTLE vesicles and SS Aβ oligomers (Figure 5), and subsequent disintegration of the pre-formed BTLE bilayer after its exposure to SS Aβ oligomers (Figure 7) involves Aβ–lipid complex formation, a result of Aβ induced lipid extraction.

Our study clearly shows that Aβ oligomers of different sizes interact differently with the BTLE membrane. Previous studies revealed that the degree of aggregation affects both the secondary structure of amyloid molecules forming these aggregates and the number of hydrophobic sites available on the aggregate surface.[57,58] LMW Aβ oligomers are more hydrophobic than HMW Aβ oligomers.[57] Moreover, there is a clear correlation between hydrophobicity and toxicity of Aβ oligomers of different sizes.[59] That is, the higher the availability of hydrophobic sites on the aggregate surface, the higher is their toxicity. High hydrophobicity of LMW oligomers is the reason for their instability in polar solvent solutions. In these solutions, individual amyloid molecules spontaneously aggregate and minimize the number of exposed hydrophobic residues. However, in the presence of a biological membrane LMW Aβ oligomers adsorb on the membrane surface. In the adsorbed state, LMW Aβ oligomers preferentially interact with hydrophobic phospholipid chains to form stable lipid–Aβ complexes. In contrast, hydrophobicity of the preformed HMW Aβ oligomers is lower because they assume the β-sheet secondary structure. This secondary structure is a matrix for extending and forming fibrils by intermolecular hydrogen bonding and also by side chain interactions with other HMW oligomers.[57,58]

CONCLUSIONS

The unique direct visualization, by means of high-resolution AFM imaging, allowed distinguishing between two different mechanisms of interaction of various size Aβ oligomers with a model brain-like phospholipid membrane. LS Aβ oligomers aggregated on the BTLE bilayer surface via both primary and secondary nucleation mechanisms, but the surface integrity of the bilayer remained intact. Unlike the LS Aβ oligomers, SS Aβ oligomers destroyed the BTLE bilayer. The destruction mechanism consisted of two consecutive events, that is, pore

DOI: 10.1021/acs.langmuir.9b01645
Langmuir 2019, 35, 11940–11949

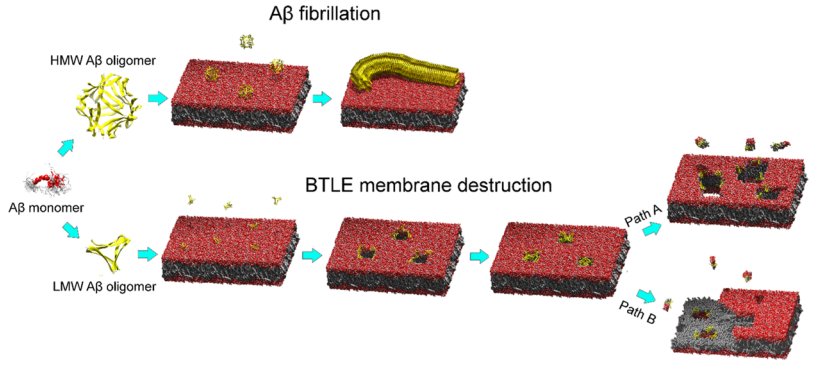

Figure 8. Illustration of the proposed mechanisms of the LS and SS Aβ oligomer interaction with the BTLE bilayer. The scheme was produced in UCSF Chimera software[60] using PDB files 2OMPF,[61] 1Z0Q,[62] 5V63,[63] and 5KK3,[64] for lipid bilayer, Aβ monomer, SS, and LS Aβ oligomers and Aβ fibril, respectively.

formation followed by lipid extraction. After pore formation, first, the pores expanded over time, and then SS Aβ oligomers inserted themselves into these pores. The next step involved the extraction of phospholipid molecules from the membrane leading to the formation of Aβ–lipid complexes. Lipid extraction from the membrane, most likely, proceeds either via simultaneous involvement of phospholipids from both bilayer leaflets or, first, phospholipids from the outer, and then, from the inner leaflet are extracted. Figure 8 illustrates the proposed mechanisms of Aβ fibrillation and BTLE membrane destruction.

Both SS and LS Aβ oligomers cause a ~50% decrease in the bilayers YM. This decrease indicates that both forms of Aβ oligomers affect membrane stability but each in a different way. This should lead to differences in the toxicity and this should be investigated in future cytotoxicity studies.

Our results explain the mechanisms of toxicity of Aβ oligomers at different stages of aggregation and reconcile contradictory reports published in the literature. Moreover, our findings well correlate with the two distinct features found in AD patients, that is, simultaneous presence of amyloid plaques in their brains and pathological consequences of neuronal death. The differences in the mechanism of SS and LS Aβ oligomer interaction with a model cell membrane suggest that each of the oligomer forms may require unique treatment to inhibit their toxicity.

■ ASSOCIATED CONTENT

Supporting Information

The Supporting Information is available free of charge on the ACS Publications website at DOI: 10.1021/acs.langmuir.9b01645.

NMR spectra, additional AFM images, statistical analysis of sizes, and AFM tip characterization (PDF)

Entry of Aβ oligomers into a single pore (MP4)

Entry of Aβ oligomers into multiple pores and pores expansion (MP4)

■ AUTHOR INFORMATION

Corresponding Author

*E-mail: ppieta@ichf.edu.pl.

ORCID

Izabela S. Pieta: 0000-0002-3394-7116

Piotr Bernatowicz: 0000-0001-8891-0380

Wlodzimierz Kutner: 0000-0003-3586-5170

Jacek Lipkowski: 0000-0001-6449-7464

Piotr Pieta: 0000-0003-0341-2310

Notes

The authors declare no competing financial interest.

■ ACKNOWLEDGMENTS

This research was supported by receiving funding from Polish National Science Centre, grant no. OPUS12 2016/23/B/ST4/02791, and the European Union Horizon 2020 Research and Innovation Programme under the Marie Skłodowska-Curie grant agreement no. 711859 and the Polish Ministry of Science and Higher Education for the implementation of an international co-financed project in the years 2017–2021.

■ REFERENCES

(1) Cummings, J. L. Alzheimer's Disease. *N. Engl. J. Med.* **2004**, *351*, 56–67.

(2) Chaudhuri, T. K.; Paul, S. Protein-Misfolding Diseases and Chaperone-Based Therapeutic Approaches. *FEBS J.* **2006**, *273*, 1331–1349.

(3) LaFerla, F. M.; Green, K. N.; Oddo, S. Intracellular Amyloid-β in Alzheimer's Disease. *Nat. Rev. Neurosci.* **2007**, *8*, 499–509.

(4) Vassar, R.; Bennett, B. D.; Babu-Khan, S.; Kahn, S.; Mendiaz, E. A.; Denis, P.; Teplow, D. B.; Ross, S.; Amarante, P.; Loeloff, R.; et al. β-Secretase Cleavage of Alzheimer's Amyloid Precursor Protein by the Transmembrane Aspartic Protease BACE. *Science* **1999**, *286*, 735–741.

(5) Allan Butterfield, D.; Swomley, A. M.; Sultana, R. Amyloid β-Peptide (1-42)-Induced Oxidative Stress in Alzheimer Disease: Importance in Disease Pathogenesis and Progression. *Antioxid. Redox Signaling* **2013**, *19*, 823–835.

(6) Walsh, D. M.; Lomakin, A.; Benedek, G. B.; Condron, M. M.; Teplow, D. B. Amyloid β-Protein Fibrillogenesis. *J. Biol. Chem.* **1997**, *272*, 22364–22372.

(7) Kotler, S. A.; Walsh, P.; Brender, J. R.; Ramamoorthy, A. Differences between Amyloid-β Aggregation in Solution and on the Membrane: Insights into Elucidation of the Mechanistic Details of Alzheimer's Disease. *Chem. Soc. Rev.* **2014**, *43*, 6692–6700.

(8) Lin, H.; Bhatia, R.; Lal, R. Amyloid β protein forms ion channels: implications for Alzheimer's disease pathophysiology. *FASEB J.* **2001**, *15*, 2433–2444.

(9) Quist, A.; Doudevski, I.; Lin, H.; Azimova, R.; Ng, D.; Frangione, B.; Kagan, B.; Ghiso, J.; Lal, R. Amyloid Ion Channels: A Common Structural Link for Protein-Misfolding Disease. *Proc. Natl. Acad. Sci. U.S.A.* **2005**, *102*, 10427–10432.

(10) Delgado, D. A.; Doherty, K.; Cheng, Q.; Kim, H.; Xu, D.; Dong, H.; Grewer, C.; Qiang, W. Distinct Membrane Disruption Pathways Are Induced by 40-Residue β-Amyloid Peptides. *J. Biol. Chem.* **2016**, *291*, 12233–12244.

DOI: 10.1021/acs.langmuir.9b01645
Langmuir 2019, 35, 11940–11949

(11) Sciacca, M. F. M.; Kotler, S. A.; Brender, J. R.; Chen, J.; Lee, D.-K.; Ramamoorthy, A. Two-Step Mechanism of Membrane Disruption by Aβ through Membrane Fragmentation and Pore Formation. *Biophys. J.* **2012**, *103*, 702−710.
(12) Sokolov, Y.; Kozak, J. A.; Kayed, R.; Chanturiya, A.; Glabe, C.; Hall, J. E. Soluble Amyloid Oligomers Increase Bilayer Conductance by Altering Dielectric Structure. *J. Gen. Physiol.* **2006**, *128*, 637−647.
(13) Tofoleanu, F.; Buchete, N.-V. Molecular Interactions of Alzheimer's Aβ Protofilaments with Lipid Membranes. *J. Mol. Biol.* **2012**, *421*, 572−586.
(14) Treusch, S.; Cyr, D. M.; Lindquist, S. Amyloid Deposits: Protection against Toxic Protein Species? *Cell Cycle* **2009**, *8*, 1668−1674.
(15) Vácha, R.; Linse, S.; Lund, M. Surface Effects on Aggregation Kinetics of Amyloidogenic Peptides. *J. Am. Chem. Soc.* **2014**, *136*, 11776−11782.
(16) Moores, B.; Drolle, E.; Attwood, S. J.; Simons, J.; Leonenko, Z. Effect of Surfaces on Amyloid Fibril Formation. *PLoS One* **2011**, *6*, No. e25954.
(17) Lee, J.; Kim, Y. H.; Arce, F. T.; Gillman, H.; Kagan, B. L.; Nussinov, R.; Yang, J.; Lal, R.; Lal, R. Amyloid β Ion Channels in a Membrane Comprising Brain Total Lipid Extracts. *ACS Chem. Neurosci.* **2017**, *8*, 1348−1357.
(18) Dante, S.; Hauß, T.; Steitz, R.; Canale, C.; Dencher, N. A. Nanoscale structural and mechanical effects of beta-amyloid (1-42) on polymer cushioned membranes: A combined study by neutron reflectometry and AFM Force Spectroscopy. *Biochim. Biophys. Acta, Biomembr.* **2011**, *1808*, 2646−2655.
(19) Jao, S.-C.; Ma, K.; Talafous, J.; Orlando, R.; Zagorski, M. G. Trifluoroacetic acid pretreatment reproducibly disaggregates the amyloid β-peptide. *Amyloid* **1997**, *4*, 240−252.
(20) Stine, W. B.; Jungbauer, L.; Yu, C.; LaDu, M. J. Preparing Synthetic Aβ in Different Aggregation States. In *Alzheimer's Disease and Frontotemporal Dementia: Methods and Protocols*; Roberson, E. D., Ed.; Humana Press: Totowa, NJ, United States, 2010; Vol. *670*, pp 13−32.
(21) Banerjee, S.; Hashemi, M.; Lv, Z.; Maity, S.; Rochet, J.-C.; Lyubchenko, Y. L. A Novel Pathway for Amyloids Self-Assembly in Aggregates at Nanomolar Concentration Mediated by the Interaction with Surfaces. *Sci. Rep.* **2017**, *7*, 45592.
(22) Chromy, B. A.; Nowak, R. J.; Lambert, M. P.; Viola, K. L.; Chang, L.; Velasco, P. T.; Jones, B. W.; Fernandez, S. J.; Lacor, P. N.; Horowitz, P.; et al. Self-Assembly of Aβ1-42 into Globular Neurotoxins. *Biochemistry* **2003**, *42*, 12749−12760.
(23) McConnell, H. M.; Watts, T. H.; Weis, R. M.; Brian, A. A. Supported Planar Membranes in Studies of Cell-Cell Recognition in the Immune System. *Biochim. Biophys. Acta, Rev. Biomembr.* **1986**, *864*, 95−106.
(24) Gurtovenko, A. A.; Anwar, J. Modulating the Structure and Properties of Cell Membranes: The Molecular Mechanism of Action of Dimethyl Sulfoxide. *J. Phys. Chem. B* **2007**, *111*, 10453−10460.
(25) Notman, R.; Noro, M.; O'Malley, B.; Anwar, J. Molecular Basis for Dimethylsulfoxide (DMSO) Action on Lipid Membranes. *J. Am. Chem. Soc.* **2006**, *128*, 13982−13983.
(26) Hutter, J. L.; Bechhoefer, J. Calibration of Atomic-force Microscope Tips. *Rev. Sci. Instrum.* **1993**, *64*, 1868−1873.
(27) Lévy, R.; Maaloum, M. Measuring the Spring Constant of Atomic Force Microscope Cantilevers: Thermal Fluctuations and Other Methods. *Nanotechnology* **2002**, *13*, 33−37.
(28) Nečas, D.; Klapetek, P. Gwyddion: An Open-Source Software for SPM Data Analysis. *Open Phys.* **2012**, *10*, 181−188.
(29) Hermanowicz, P.; Sarna, M.; Burda, K.; Gabryś, H. AtomicJ: An Open Source Software for Analysis of Force Curves. *Rev. Sci. Instrum.* **2014**, *85*, 063703.
(30) Vold, R. L.; Waugh, J. S.; Klein, M. P.; Phelps, D. E. Measurement of Spin Relaxation in Complex Systems. *J. Chem. Phys.* **1968**, *48*, 3831−3832.
(31) Attwood, S.; Choi, Y.; Leonenko, Z. Preparation of DOPC and DPPC Supported Planar Lipid Bilayers for Atomic Force Microscopy and Atomic Force Spectroscopy. *Int. J. Mol. Sci.* **2013**, *14*, 3514−3539.
(32) Milhiet, P.-E.; Gubellini, F.; Berquand, A.; Dosset, P.; Rigaud, J.-L.; Le Grimellec, C.; Lévy, D. High-Resolution AFM of Membrane Proteins Directly Incorporated at High Density in Planar Lipid Bilayer. *Biophys. J.* **2006**, *91*, 3268−3275.
(33) Ono, K.; Condron, M. M.; Teplow, D. B. Structure-Neurotoxicity Relationships of Amyloid β-Protein Oligomers. *Proc. Natl. Acad. Sci. U.S.A.* **2009**, *106*, 14745−14750.
(34) Cizas, P.; Budvytyte, R.; Morkuniene, R.; Moldovan, R.; Broccio, M.; Lösche, M.; Niaura, G.; Valincius, G.; Borutaite, V. Size-dependent neurotoxicity of β-amyloid oligomers. *Arch. Biochem. Biophys.* **2010**, *496*, 84−92.
(35) Chimon, S.; Shaibat, M. A.; Jones, C. R.; Calero, D. C.; Aizezi, B.; Ishii, Y. Evidence of fibril-like β-sheet structures in a neurotoxic amyloid intermediate of Alzheimer's β-amyloid. *Nat. Struct. Mol. Biol.* **2007**, *14*, 1157−1164.
(36) Dahlgren, K. N.; Manelli, A. M.; Stine, W. B.; Baker, L. K.; Krafft, G. A.; LaDu, M. J. Oligomeric and Fibrillar Species of Amyloid-β Peptides Differentially Affect Neuronal Viability. *J. Biol. Chem.* **2002**, *277*, 32046−32053.
(37) Nag, S.; Sarkar, B.; Bandyopadhyay, A.; Sahoo, B.; Sreenivasan, V. K. A.; Kombrabail, M.; Muralidharan, C.; Maiti, S. Nature of the Amyloid-β Monomer and the Monomer-Oligomer Equilibrium. *J. Biol. Chem.* **2011**, *286*, 13827−13833.
(38) Blaine Stine, W.; Dahlgren, K. N.; Krafft, G. A.; LaDu, M. J. In Vitro Characterization of Conditions for Amyloid-β Peptide Oligomerization and Fibrillogenesis. *J. Biol. Chem.* **2003**, *278*, 11612−11622.
(39) Bitan, G.; Kirkitadze, M. D.; Lomakin, A.; Vollers, S. S.; Benedek, G. B.; Teplow, D. B. Amyloid β-Protein (Aβ) Assembly: Aβ 40 and Aβ 42 Oligomerize through Distinct Pathways. *Proc. Natl. Acad. Sci. U.S.A.* **2003**, *100*, 330−335.
(40) Bartolini, M.; Naldi, M.; Fiori, J.; Valle, F.; Biscarini, F.; Nicolau, D. V.; Andrisano, V. Kinetic Characterization of Amyloid-Beta 1-42 Aggregation with a Multimethodological Approach. *Anal. Biochem.* **2011**, *414*, 215−225.
(41) Ahmed, M.; Davis, J.; Aucoin, D.; Sato, T.; Ahuja, S.; Aimoto, S.; Elliott, J. I.; Van Nostrand, W. E.; Smith, S. O. Structural conversion of neurotoxic amyloid-β1-42 oligomers to fibrils. *Nat. Struct. Mol. Biol.* **2010**, *17*, 561−567.
(42) Roher, A. E.; Chaney, M. O.; Kuo, Y.-M.; Webster, S. D.; Stine, W. B.; Haverkamp, L. J.; Woods, A. S.; Cotter, R. J.; Tuohy, J. M.; Krafft, G. A.; et al. Morphology and Toxicity of Aβ-(1-42) Dimer Derived from Neuritic and Vascular Amyloid Deposits of Alzheimer's Disease. *J. Biol. Chem.* **1996**, *271*, 20631−20635.
(43) Lindberg, D. J.; Wesén, E.; Björkeroth, J.; Rocha, S.; Esbjörner, E. K. Lipid membranes catalyse the fibril formation of the amyloid-β (1-42) peptide through lipid-fibril interactions that reinforce secondary pathways. *Biochim. Biophys. Acta, Biomembr.* **2017**, *1859*, 1921−1929.
(44) Habchi, J.; Chia, S.; Galvagnion, C.; Michaels, T. C. T.; Bellaiche, M. M. J.; Ruggeri, F. S.; Sanguanini, M.; Idini, I.; Kumita, J. R.; Sparr, E.; et al. Cholesterol catalyses Aβ42 aggregation through a heterogeneous nucleation pathway in the presence of lipid membranes. *Nat. Chem.* **2018**, *10*, 673−683.
(45) Aisenbrey, C.; Borowik, T.; Byström, R.; Bokvist, M.; Lindström, F.; Misiak, H.; Sani, M.-A.; Gröbner, G. How Is Protein Aggregation in Amyloidogenic Diseases Modulated by Biological Membranes? *Eur. Biophys. J.* **2008**, *37*, 247−255.
(46) Chi, E. Y.; Ege, C.; Winans, A.; Majewski, J.; Wu, G.; Kjaer, K.; Lee, K. Y. C. Lipid membrane templates the ordering and induces the fibrillogenesis of Alzheimer's disease amyloid-β peptide. *Proteins: Struct., Funct., Bioinf.* **2008**, *72*, 1−24.
(47) Cohen, S. I. A.; Linse, S.; Luheshi, L. M.; Hellstrand, E.; White, D. A.; Rajah, L.; Otzen, D. E.; Vendruscolo, M.; Dobson, C. M.; Knowles, T. P. J. Proliferation of Amyloid-β42 Aggregates Occurs

DOI: 10.1021/acs.langmuir.9b01645
Langmuir 2019, 35, 11940−11949

through a Secondary Nucleation Mechanism. *Proc. Natl. Acad. Sci. U.S.A.* **2013**, *110*, 9758−9763.
(48) Michikawa, M.; Gong, J.-S.; Fan, Q.-W.; Sawamura, N.; Yanagisawa, K. A Novel Action of Alzheimer's Amyloid β-Protein (Aβ): Oligomeric Aβ Promotes Lipid Release. *J. Neurosci.* **2001**, *21*, 7226−7235.
(49) Butterfield, S. M.; Lashuel, H. A. Amyloidogenic Protein-Membrane Interactions: Mechanistic Insight from Model Systems. *Angew. Chem., Int. Ed.* **2010**, *49*, 5628−5654.
(50) Nakazawa, Y.; Suzuki, Y.; Williamson, M. P.; Saitô, H.; Asakura, T. The interaction of amyloid Aβ(1-40) with lipid bilayers and ganglioside as studied by 31P solid-state NMR. *Chem. Phys. Lipids* **2009**, *158*, 54−60.
(51) Tashima, Y.; Oe, R.; Lee, S.; Sugihara, G.; Chambers, E. J.; Takahashi, M.; Yamada, T. The Effect of Cholesterol and Monosialoganglioside (GM1) on the Release and Aggregation of Amyloid β-Peptide from Liposomes Prepared from Brain Membrane-like Lipids. *J. Biol. Chem.* **2004**, *279*, 17587−17595.
(52) Cohen, S. I. A.; Cukalevski, R.; Michaels, T. C. T.; Šarić, A.; Törnquist, M.; Vendruscolo, M.; Dobson, C. M.; Buell, A. K.; Knowles, T. P. J.; Linse, S. Distinct thermodynamic signatures of oligomer generation in the aggregation of the amyloid-β peptide. *Nat. Chem.* **2018**, *10*, 523−531.
(53) Kroemer, G.; Jäättelä, M. Lysosomes and Autophagy in Cell Death Control. *Nat. Rev. Cancer* **2005**, *5*, 886−897.
(54) Rosales-Corral, S.; Acuna-Castroviejo, D.; Tan, D. X.; López-Armas, G.; Cruz-Ramos, J.; Munoz, R.; Melnikov, V. G.; Manchester, L. C.; Reiter, R. J. Accumulation of Exogenous Amyloid-Beta Peptide in Hippocampal Mitochondria Causes Their Dysfunction: A Protective Role for Melatonin. *Oxid. Med. Cell. Longevity* **2012**, *2012*, 1−15.
(55) Domínguez-Prieto, M.; Velasco, A.; Tabernero, A.; Medina, J. M. Endocytosis and Transcytosis of Amyloid-β Peptides by Astrocytes: A Possible Mechanism for Amyloid-β Clearance in Alzheimer's Disease. *J. Alzheimer's Dis.* **2018**, *65*, 1109−1124.
(56) Tseng, B. P.; Green, K. N.; Chan, J. L.; Blurton-Jones, M.; LaFerla, F. M. Aβ inhibits the proteasome and enhances amyloid and tau accumulation. *Neurobiol. Aging* **2008**, *29*, 1607−1618.
(57) Fu, Z.; Aucoin, D.; Davis, J.; Van Nostrand, W. E.; Smith, S. O. Mechanism of Nucleated Conformational Conversion of Aβ42. *Biochemistry* **2015**, *54*, 4197−4207.
(58) Fu, Z.; Aucoin, D.; Ahmed, M.; Ziliox, M.; Van Nostrand, W. E.; Smith, S. O. Capping of Aβ42 Oligomers by Small Molecule Inhibitors. *Biochemistry* **2014**, *53*, 7893−7903.
(59) Bolognesi, B.; Kumita, J. R.; Barros, T. P.; Esbjorner, E. K.; Luheshi, L. M.; Crowther, D. C.; Wilson, M. R.; Dobson, C. M.; Favrin, G.; Yerbury, J. J. ANS Binding Reveals Common Features of Cytotoxic Amyloid Species. *ACS Chem. Biol.* **2010**, *5*, 735−740.
(60) Pettersen, E. F.; Goddard, T. D.; Huang, C. C.; Couch, G. S.; Greenblatt, D. M.; Meng, E. C.; Ferrin, T. E. UCSF Chimera-A Visualization System for Exploratory Research and Analysis. *J. Comput. Chem.* **2004**, *25*, 1605−1612.
(61) Tieleman, D. P.; Berendsen, H. J. C. A Molecular Dynamics Study of the Pores Formed by Escherichia Coli OmpF Porin in a Fully Hydrated Palmitoyloleoylphosphatidylcholine Bilayer. *Biophys. J.* **1998**, *74*, 2786−2801.
(62) Tomaselli, S.; Esposito, V.; Vangone, P.; van Nuland, N. A. J.; Bonvin, A. M. J. J.; Guerrini, R.; Tancredi, T.; Temussi, P. A.; Picone, D. The α-to-β Conformational Transition of Alzheimer's Aβ-(1-42) Peptide in Aqueous Media is Reversible: A Step by Step Conformational Analysis Suggests the Location of β Conformation Seeding. *ChemBioChem* **2006**, *7*, 257−267.
(63) Salveson, P. J.; Spencer, R. K.; Kreutzer, A. G.; Nowick, J. S. X-ray Crystallographic Structure of a Compact Dodecamer from a Peptide Derived from Aβ 16-36. *Org. Lett.* **2017**, *19*, 3462−3465.
(64) Colvin, M. T.; Silvers, R.; Ni, Q. Z.; Can, T. V.; Sergeyev, I.; Rosay, M.; Donovan, K. J.; Michael, B.; Wall, J.; Linse, S.; et al. Atomic Resolution Structure of Monomorphic Aβ42 Amyloid Fibrils. *J. Am. Chem. Soc.* **2016**, *138*, 9663−9674.

DOI: 10.1021/acs.langmuir.9b01645
Langmuir 2019, 35, 11940−11949